ELECTRONIC SUPPLEMENTARY INFORMATION

Polyoxometalates as alternative Mo precursors for methane dehydroaromatization on Mo/ZSM-5 and Mo/MCM-22 catalysts

Ignacio Julian*, Jose L. Hueso, Nidya Lara, Albert Sole-Daura, Josep M. Poblet, Scott G. Mitchell*, Reyes Mallada, Jesus Santamaria

CONTENTS

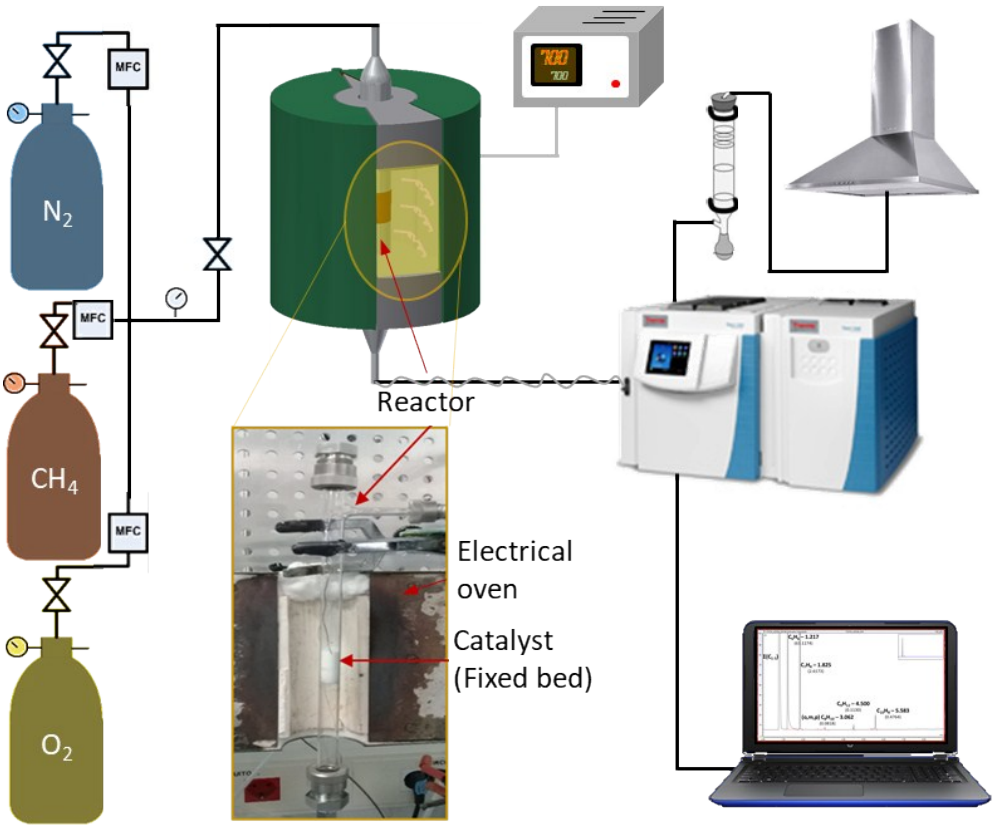

Figure S1. Experimental set-up for methane dehydroaromatization tests

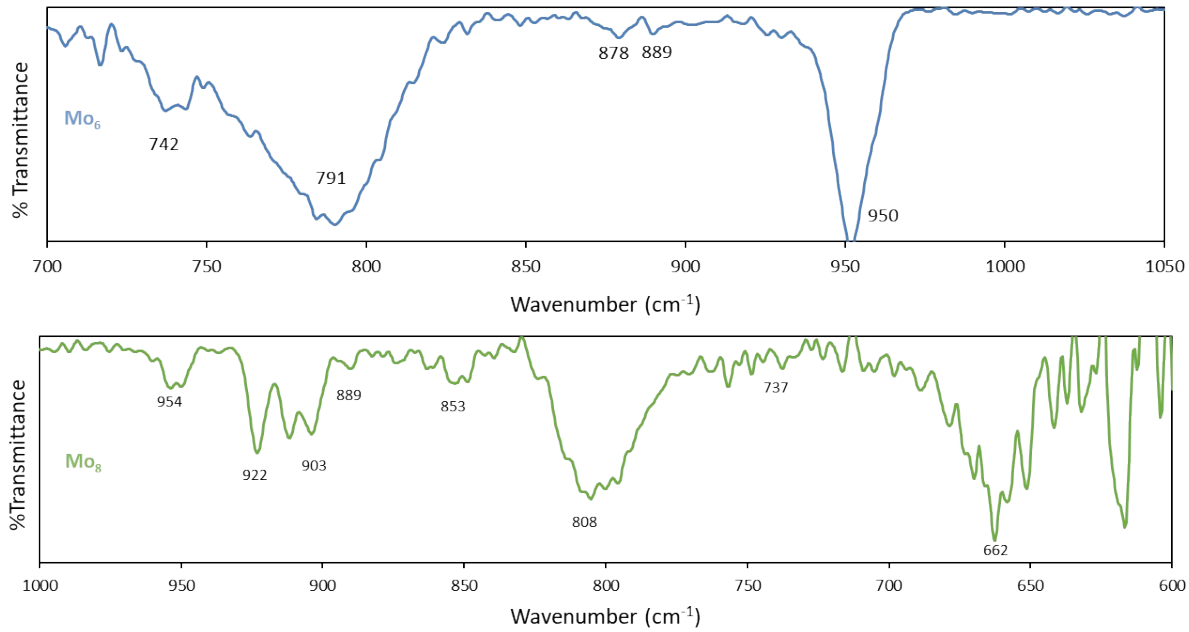

Figure S2. FTIR spectra of fresh polyoxometalates Mo_6 and Mo_8, as precursors of Mo/ZSM-5 and Mo/MCM-22 catalysts

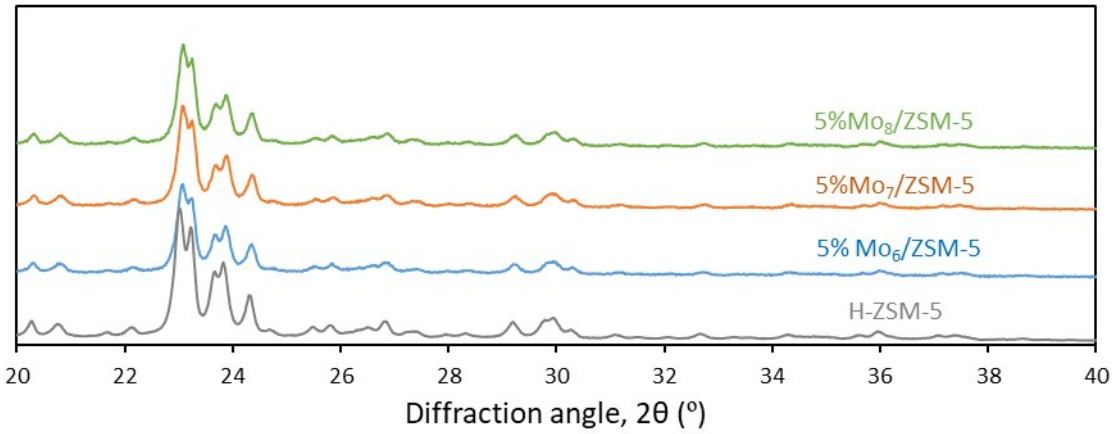

Figure S3. XRD of calcined Mo/ZSM-5 catalysts in air at 550ºC during 6 hours, containing 5% Mo from hexa-, hepta- and octamolybdate precursors. The crystalline structure of the ZSM-5 does not change with the addition of 5% Mo regardless of the employed precursor

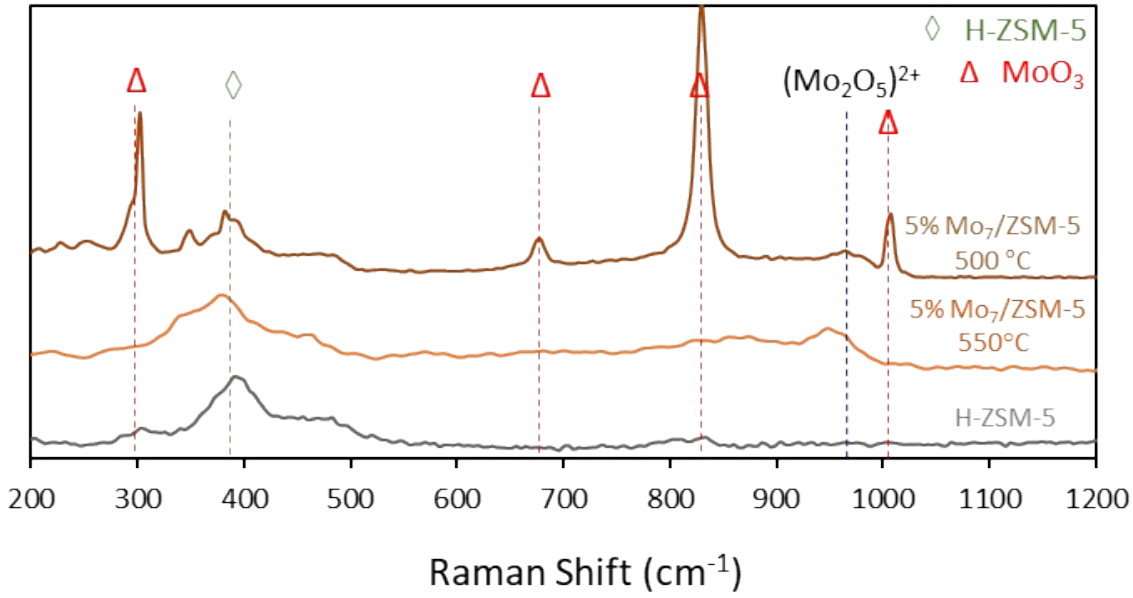

Figure S4. Raman shift of fresh ZSM-5 and calcined 5%Mo_7/ZSM-5 in air for 6 hours at two different temperatures, 500 and 550°C. The sample calcined at 500°C contains external MoO_3 species (characteristic bands at 670, 820 and 1000 cm^{-1}) whereas the calcination at 550°C produces the diffusion of MoO_x through the channels and the anchoring of $[Mo_2O_5]^{2+}$ species at the Brønsted sites

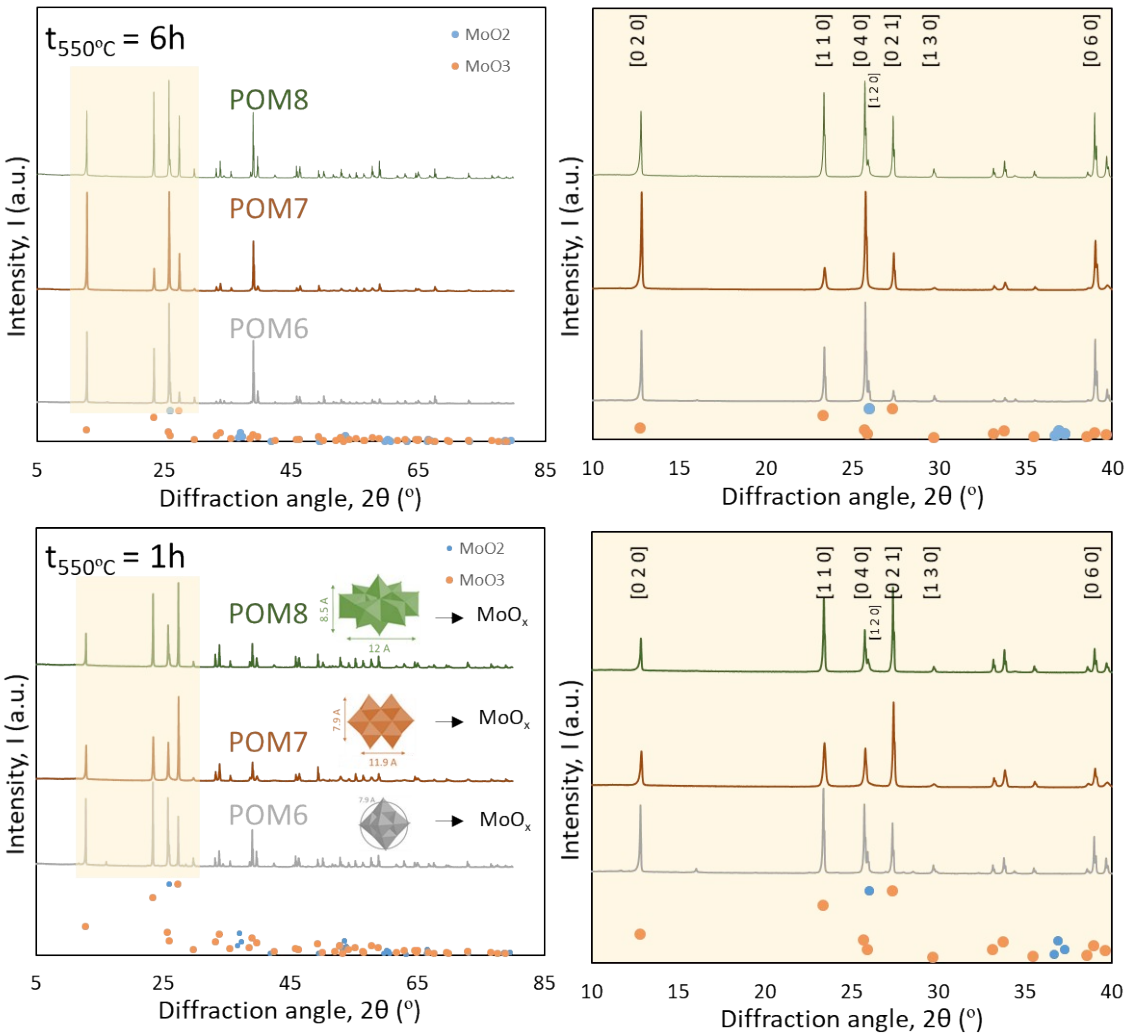

Figure S5. XRD diffractograms of calcined hexa-, hepta- and octamolybdates (POM6, 7 and 8) in air at 550°C for 1 and 6 hours. The yellow background represents a zoom to diffraction angles in the range 10° - 40°. The oxidation of the Mo species into MoO_{3-x} proceeds differently for each sample and the resulting oxidation state and crystal size differs consequently.

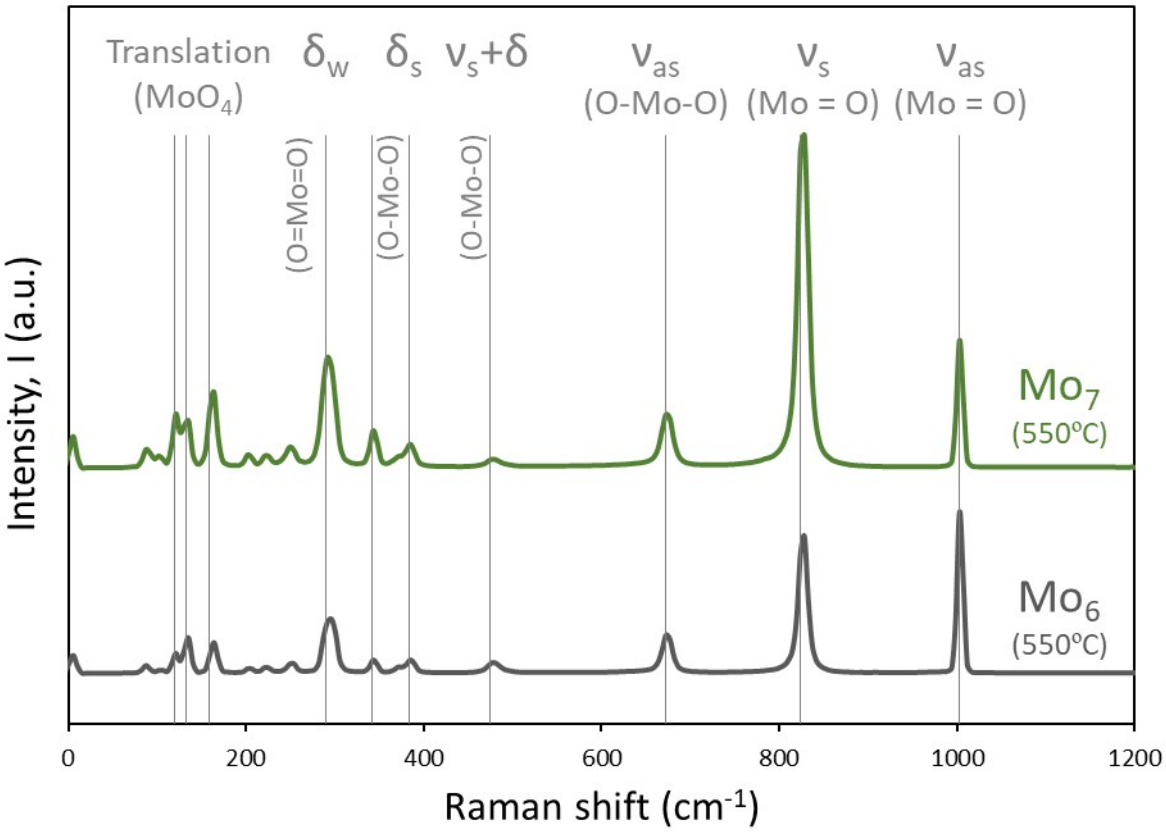

Figure S6. Raman spectra of hexa- and heptamolybdate precursors calcined in air at 550ºC for 6 hours. The differences in the relative intensity between the characteristic symmetric (823 cm^{-1}) and anti-symmetric (1004 cm^{-1}) stretching bands of the Mo = O bond reveals the presence of different MoO_x structure arrangements

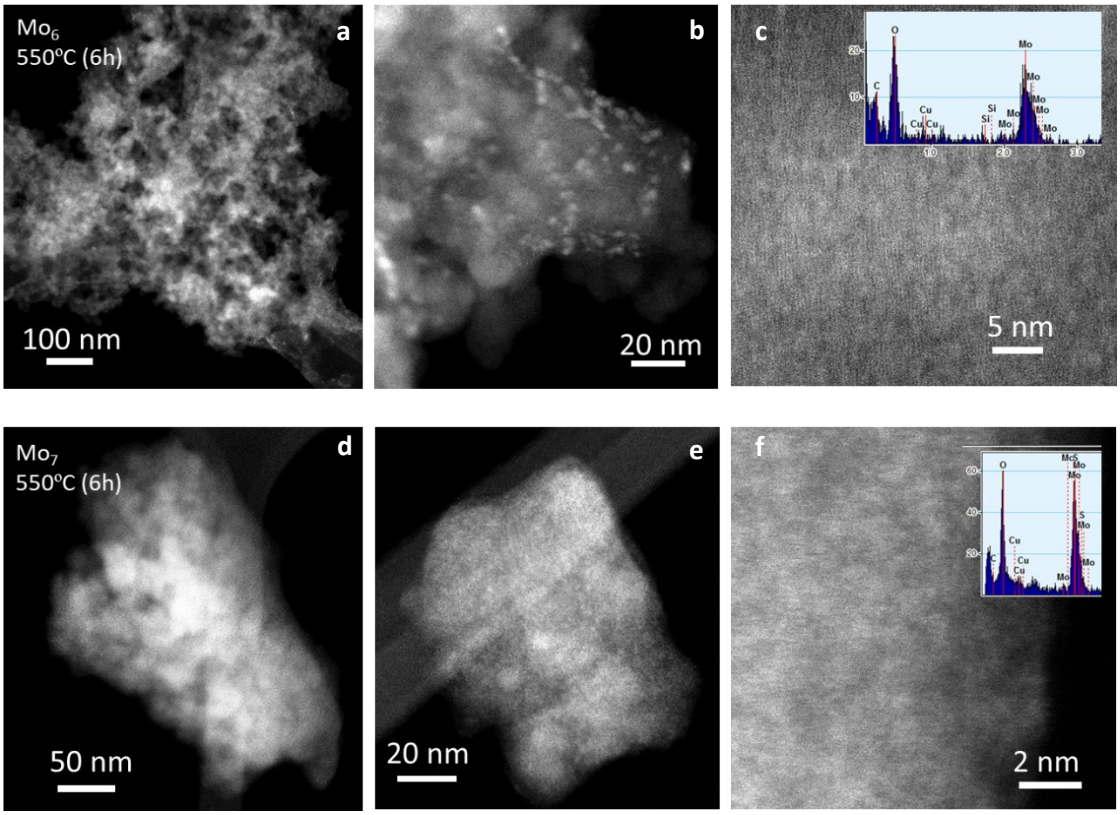

Figure S7. STEM-HAADF micrographs of hexa- (**a** – **c**) and heptamolybdate (**d** – **f**) precursors calcined in air at 550ºC for 6 hours. The calcined Mo_6 adopts a somehow more ordered structure during the calcination step, attending to the oriented planes observed in **c** and their absence in **f**

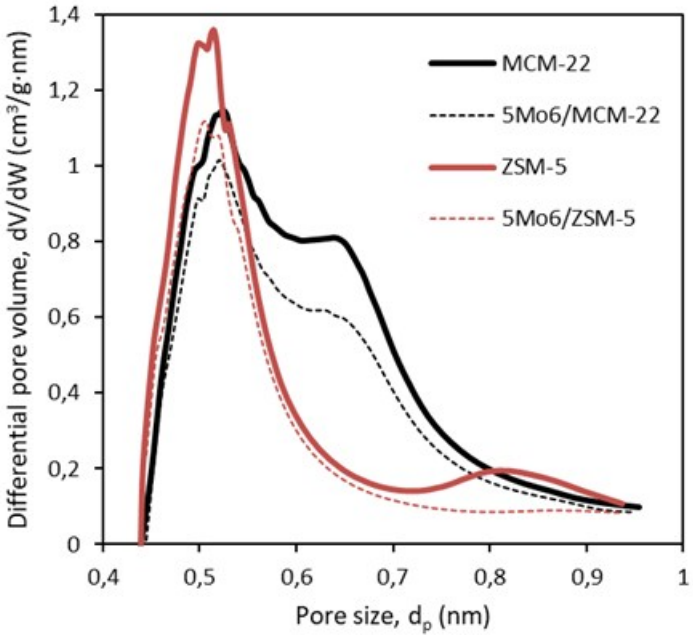

Figure S8. Pore size distribution of fresh supports (ZSM-5 and MCM-22) and Mo-based catalysts using hexamolybdate as Mo precursor

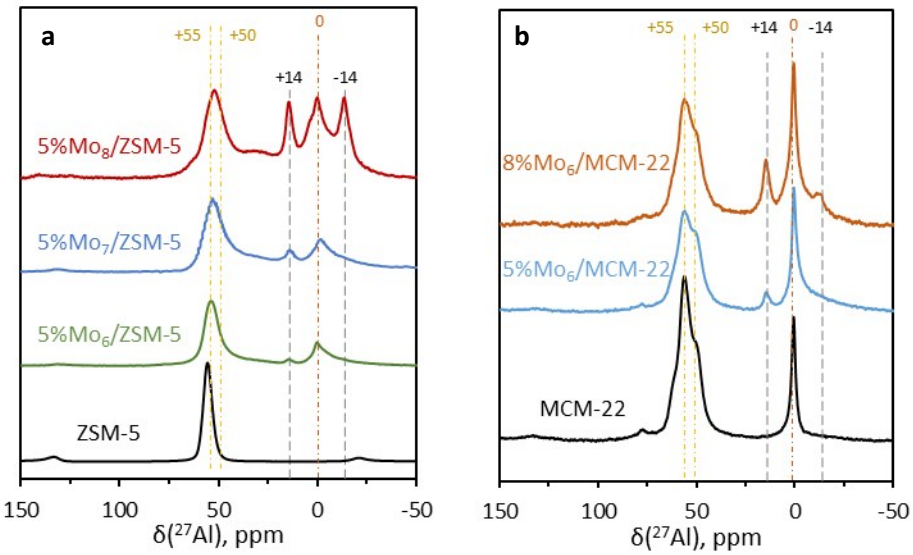

Figure S9. ^{27}Al MAS NMR of the catalytic samples to illustrate both the effect of the metal precursor (a) and metal load (b) on the final structure of the catalysts

ADDITIONAL DISCUSSION ON NMR RESULTS:

The band at 0 ppm indicates the presence of extra-framework octahedral aluminium. The chemical shifts at 50 and 55 ppm belong to framework tetrahedral aluminium. The shifts at +14 and -14 are attributed to the hydrated and (resonant) non-hydrated forms of the aluminium molybdate phase, i.e. $[Al(OH)_n(H_2O)_{6-n}]_n(MoO_4)$ (n = 1 or 2) and $Al_2(MoO_4)_3$, respectively[S1]. The last species appear as a result of a strong interaction between the molybdenum and the zeolite aluminium species. According to this, the use of Mo_8 as precursor was detrimental for the synthesis of 5%Mo/ZSM-5 since it led to significant dealuminization of the ZSM-5 framework and to the generation of $Al_2(MoO_4)_3$ crystallites. The coexistence of hydrated and non-hydrated $Al_2(MoO_4)_3$ crystallites suggests that this species is also present in the bulk and not only at the catalyst surface[S1]. The spectra of 5%Mo_6/ZSM-5 and 5%Mo_7/ZSM-5, however, are very similar and indicate a substantially lower presence of extra-framework aluminium and aluminium molybdate. Nevertheless, the bands at 0 and +14 ppm and at the range 50 – 55 ppm are slightly greater and broader, respectively, in the case of 5%Mo_7/ZSM-5. This would indicate a slightly greater dealuminization and the presence of a greater number of $Al_2(MoO_4)_3$ species at the catalyst surface.

The previous discussion applies to evaluate the effect of Mo loading on the Mo_6/MCM-22 catalysts. The greater the Mo content, the more intense are the peaks related to extra-framework octahedral Al (0 ppm) and aluminium molybdate (+14 ppm). The appearance of the peak of non-hydrated $Al_2(MoO_4)_3$ at -14 ppm for the 8%Mo_6/MCM-22 catalyst is again attributed to the presence of bulk aluminium molybdate apart from that at the surface. The as-synthesized MCM-22 zeolite was found to have a contribution of both aluminium species with tetrahedral (50 – 55 ppm) and octahedral (0 ppm) coordination, as already reported in literature[S1].

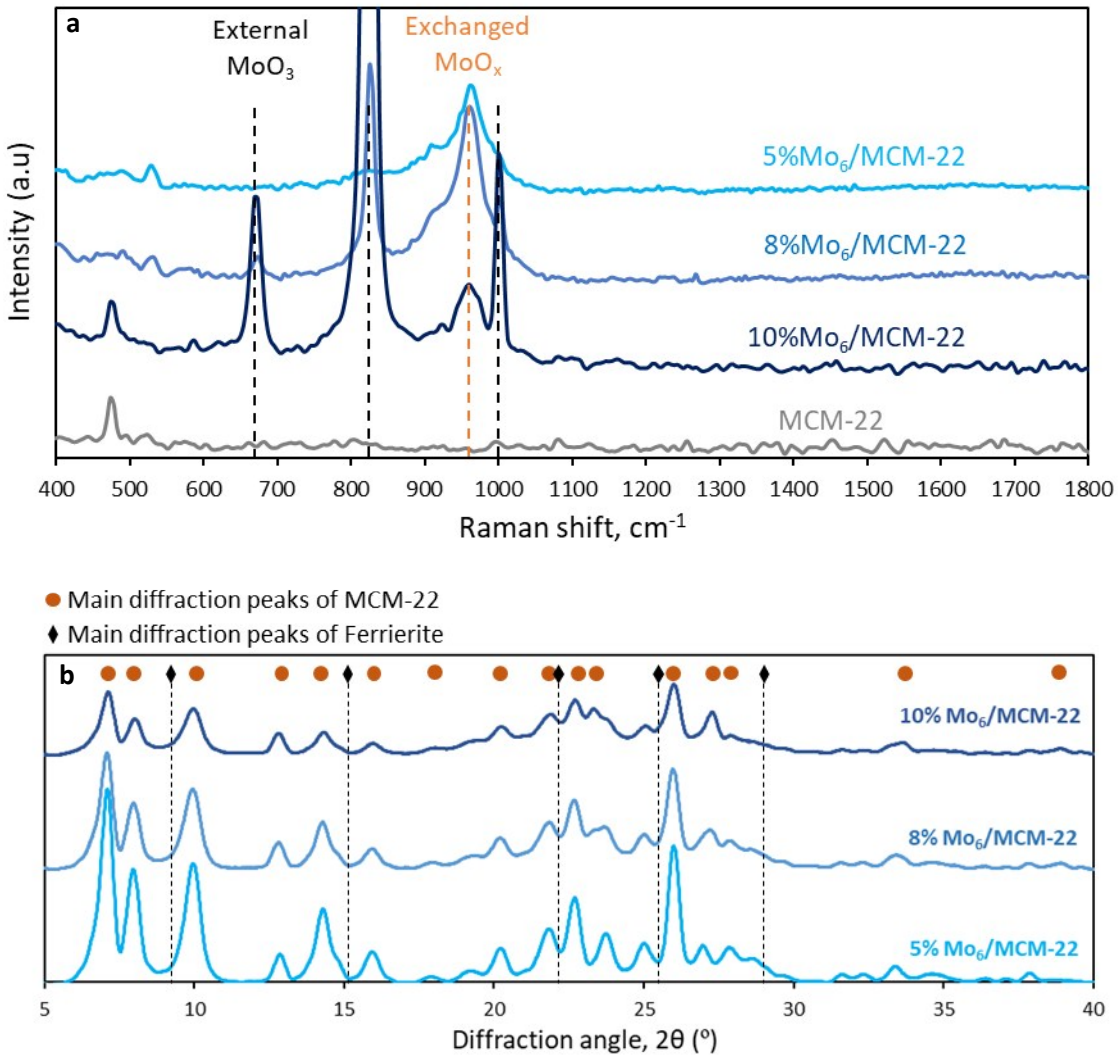

Figure S10. a) Raman shift of MCM-22 support and Mo_6-based catalysts having different metal loads. High metal loads (>5%) saturate the channels of the MCM-22 and form large MoO_3 aggregates at its external surface, as revealed by the appearance of bands around 670, 820 and 1000 cm^{-1} in the samples containing 8% and 10%Mo_6; **b)** XRD of Mo_6/MCM-22 catalysts containing 5%, 8% and 10% Mo. The crystalline structure of the MCM-22 does not change with Mo load, although diffraction peaks become less intense at higher metal content

ADDITIONAL DISCUSSION ON XRD RESULTS:

There is not any evidence on the presence of ferrierite phase in the MCM-22 support in spite of its low acidity (Si/Al < 22). This is attributed to the fact that the synthesis of the resulting gel was conducted in a stainless-steel autoclave under heating and rotation.

Computational procedure to obtain force field parameters for POMs

Initially, the structures of all of the polyoxoanions were fully optimized without symmetry constraints using the Gaussian09 package[S1] at the DFT level using the B3LYP functional.[S3] The LANL2DZ atomic basis set[S4] was used for Mo, while oxygen centers were described by an all-electron double-ζ Pople-type basis set supplemented with polarization functions.[S5] Solvent effects of water were taken into account in the geometry optimizations by means of the dielectric IEF-PCM model,[S6] as implemented in Gaussian09.[S1] Then, CHELPG atomic charges were obtained from single-point calculations in vacuo of the optimized structures. The set of Lennard-Jones parameters for Mo were taken from UFF[S7], and the bonding parameters within the POM framework were kept rigid during the simulations by means of large force contants of the same order of magnitude tan the largest in the AMBER99 force field.[S8]

Cartesian coordinates in Å and potential electronic energies in a.u. of the most representative DFT-optimised structures (B3LYP level with IEF-PCM continuum solvent model).

Mo_6: ΔE = -1835.54749 a.u.

Mo	2.347641	10.838058	-0.063164
Mo	-0.373459	8.977689	0.654827
Mo	0.170926	11.878168	2.293427
O	-0.000113	11.241535	-0.003050
O	1.555930	9.104720	0.458531
O	-0.163835	9.951247	2.344340
O	2.007720	11.401035	1.765821
O	-0.472715	8.942117	-1.298680
O	1.716962	10.390438	-1.875478
O	2.175279	12.700341	-0.587174
O	4.062126	10.521241	-0.119108
O	0.315597	12.344730	3.968274
O	-0.669762	7.327392	1.137405
Mo	-2.347648	11.646748	0.062267
Mo	0.373394	13.507180	-0.655482
Mo	-0.169752	10.607266	-2.290819
O	-1.555503	13.380412	-0.459015
O	0.164581	12.534820	-2.345349
O	-2.009520	11.084147	-1.766708
O	0.472831	13.541027	1.298169
O	-1.714751	12.093570	1.873618
O	-2.174658	9.784135	0.586835
O	-4.061965	11.963910	0.122096
O	-0.320024	10.142569	-3.965998
O	0.670717	15.158007	-1.135585

Mo_7: ΔE = -2279.89187 a.u.

Mo	6.301454	4.733621	5.197468
Mo	3.845627	4.166764	7.462331
Mo	9.185589	4.533880	8.316972
Mo	6.738975	3.959274	10.556604
Mo	8.947425	6.574013	5.745684
Mo	3.797061	5.381295	10.511719
Mo	6.303255	6.569745	8.216161
O	5.054003	5.184579	4.062226
O	2.670507	4.547503	6.231063
O	10.304629	4.724408	9.639798

O	7.918188	4.219694	11.817174
O	7.229908	3.527972	4.352218
O	3.358309	2.602561	8.053508
O	9.921497	3.329211	7.296154
O	6.012417	2.427381	10.950627
O	10.059512	5.730499	4.697817
O	2.919402	4.070054	11.257677
O	9.325393	8.272018	5.545271
O	3.120227	6.839642	11.205615
O	7.329684	6.405245	4.721720
O	2.952387	5.374378	8.768388
O	9.797306	6.208873	7.453082
O	5.468170	5.229800	11.456579
O	7.195818	7.872168	7.445060
O	5.227524	7.403561	9.327864
O	5.319764	3.514847	6.352816
O	7.887015	3.309604	9.129849
O	5.142895	5.998144	6.851943
O	7.593476	5.808434	9.372496
O	7.689471	5.157303	6.778141
O	5.240617	4.588122	9.113276

Mo_8: ΔE = -2497.80019 a.u.

Mo	2.972563	9.836693	2.431641
Mo	8.457412	10.194898	6.584762
Mo	3.050927	8.060115	5.384629
Mo	8.379483	11.970944	3.633007
Mo	5.763673	8.228213	7.442866
Mo	5.666860	11.804755	1.575676
Mo	4.919055	11.440542	5.386666
Mo	6.512126	8.591922	3.631602
O	2.419235	9.481439	4.234603
O	9.012494	10.548969	4.781776
O	6.810976	6.937595	7.903853
O	4.618920	13.095118	1.115368
O	4.746082	8.462988	8.815144
O	6.683768	11.570288	0.202853
O	6.711358	11.644246	5.436433
O	4.721121	8.383296	3.578509
O	4.171471	12.736755	6.275149
O	7.263215	7.297564	2.743559
O	1.859342	11.080673	2.001511
O	9.570277	8.950875	7.015822
O	4.530087	10.254722	1.386457
O	6.900222	9.777985	7.631994
O	2.408844	8.447729	1.579284
O	9.021393	11.584248	7.436358
O	2.457412	6.658473	4.572455
O	8.973987	13.372240	4.445086
O	4.349473	11.513263	3.670063
O	7.079963	8.519956	5.349209
O	4.457720	9.845072	6.137377
O	6.970197	10.188555	2.881290
O	1.976322	8.273369	6.716527
O	9.452982	11.757561	2.300193
O	4.608970	7.283785	6.225136
O	6.821537	12.749156	2.793003

REFERENCES

S1. Ma, D.; Su, Y.; Han, X.; Liu, X. E.; Xu, Y.; Bao, X.; Mo/HMCM-22 catalysts for methane dehydroaromatization: a multinuclear MAS NMR study, *J. Phys. Chem. B*, **2001**, *105*, 1786 − 1793.

S2. Frisch, M. J.; Trucks, G. W.; Schlegel, H. B.; Scuseria, G. E.;Robb, M. A.; Cheeseman, J. R.; Scalmani, G.; Barone, V.; Mennucci,B.; Petersson, G. A.; Nakatsuji, H.; Caricato, M.; Li, X.; Hratchian, H.P.; Izmaylov, A. F.; Bloino, J.; Zheng, G.; Sonnenberg, J. L.; Hada, M.;Ehara, M.; Toyota, K.; Fukuda, R.; Hasegawa, J.; Ishida, M.;Nakajima, T.; Honda, Y.; Kitao, O.; Nakai, H.; Vreven, T.;Montgomery, J. A., Jr.; Peralta, J. E.; Ogliaro, F.; Bearpark, M.;Heyd, J. J.; Brothers, E.; Kudin, K. N.; Staroverov, V. N.; Kobayashi,R.; Normand, J.; Raghavachari, K.; Rendell, A.; Burant, J. C.; Iyengar,S. S.; Tomasi, J.; Cossi, M.; Rega, N.; Millam, J. M.; Klene, M.; Knox,J. E.; Cross, J. B.; Bakken, V.; Adamo, C.; Jaramillo, J.; Gomperts, R.;Stratmann, R. E.; Yazyev, O.; Austin, A. J.; Cammi, R.; Pomelli, C.;Ochterski, J. W.; Martin, R. L.; Morokuma, K.; Zakrzewski, V. G.;Voth, G. A.; Salvador, P.; Dannenberg, J. J.; Dapprich, S.; Daniels, A.D.; Farkas, Ö.; Foresman, J. B.; Ortiz, J. V.; Cioslowski, J.; Fox, D. J.Gaussian 09, revision C.01; Gaussian, Inc.: Wallingford, CT, 2009

S3. (a) Lee, C.; Yang, W.; Parr, R. G. Development of the Colle-Salvetti Correlation-Energy Formula into a Functional of the Electron Density. *Phys. Rev. B: Condens. Matter Mater. Phys*. **1988**, *37*, 785−789. (b) Becke, A. D. Density-Functional Thermochemistry. III. The Role of Exact Exchange. *J. Chem. Phys.* **1993**, *98*, 5648−5652. (c) Stephens, P. J.; Devlin, F. J.; Chabalowski, C. F.; Frisch, M. J. Ab Initio Calculation of Vibrational Absorption and Circular Dichroism Spectra Using Density Functional Force Fields. *J. Phys. Chem.* **1994**, *98*, 11623−11627.

S4. Hay, P. J.; Wadt, W. R. Ab Initio Effective Core Potentials for Molecular Calculations. Potentials for the Transition Metal Atoms Sc To Hg. *J. Chem. Phys.* **1985**, *82*, 270−283.

S5. (a) Francl, M. M.; Pietro, W. J.; Hehre, W. J.; Binkley, J. S.; Gordon, M. S.; DeFrees, D. J.; Pople, J. A. Self-Consistent Molecular Orbital Methods. XXIII. A Polarization-Type Basis Set for Second-Row Elements. *J. Chem. Phys.* **1982**, *77*, 3654–3665. (b) Hehre, W. J.; Ditchfield, R.; Pople, J. A. Self—Consistent Molecular Orbital Methods. XII. Further Extensions of Gaussian—Type Basis Sets for Use in Molecular Orbital Studies of Organic Molecules. *J. Chem. Phys.* **1972**, *56*, 2257–2261. (c) Hariharan, P. C.; Pople, J. A. The Influence of Polarization Functions on Molecular Orbital Hydrogenation Energies*. Theoret. Chim. Acta* **1973**, *28*, 213–222.

S6. Cancès, E.; Mennucci, B.; Tomasi, J. A New Integral EquationFormalism for the Polarizable Continuum Model: TheoreticalBackground and Applications to Isotropic and Anisotropic Dielectrics. *J. Chem. Phys.* **1997**, *107*, 3032−3041.

S7. Rappe, A. K.; Casewit, C. J.; Colwell, K. S.; Goddard, W. A.; Skiff, W. M. UFF, a full periodic table force field for molecular mechanics and molecular dynamics simulations *J. Am. Chem. Soc.* **1992**, *114*, 10024–10035.

S8. Wang, J.; Cieplak, P.; Kollman, P. How well does a restrained electrostatic potential (RESP) model perform in calculating conformational energies of organic and biological molecules? *J. Comput. Chem.* **2000***, 21*, 1049-1074.